Journal of
Materials in Life Sciences

Vol. 4 No. 2 (2025)

Full Paper

Synthesis of Surface-Bound ZIF-8 Layers on Titania for the Photodegradation of Tetracycline

Nurhanis Khaliesah Mohamad Zamani[a], Nor Arbani Sean[a], Sheela Chandren[a,b]*

[a] Department of Chemistry, Faculty of Science, Universiti Teknologi Malaysia, 81310 UTM Johor Bahru, Johor, Malaysia.

[b] Centre for Sustainable Nanomaterials, Universiti Teknologi Malaysia, 81310 UTM Johor Bahru, Johor, Malaysia.

Article history
Received
21 October 2025
Revised
20 November 2025
Accepted
27 November 2025
Published online
30 November 2025

*Corresponding author
sheela@utm.my

Abstract

Tetracycline's presence in water systems poses significant environmental and public health concerns due to extensive pharmaceutical discharges. Accordingly, considerable research efforts have been directed toward developing efficient catalytic systems for the photodegradation and removal of tetracycline from contaminated water. Thus, in this work, a series of zeolitic imidazolate framework-8/titania (ZIF-8/TiO_2) composites were synthesized with varied precursor concentrations of zinc nitrate hexahydrate ($Zn(NO_3)_2{\cdot}6H_2O$) and 2-methylimidazole ($C_4H_6N_2$). The precursor ratios were adjusted to control the growth and distribution of ZIF-8 on TiO_2, thereby tuning its physicochemical properties and photocatalytic performance. The prepared samples were characterized by Fourier transform infrared (FTIR) spectroscopy, ultraviolet-visible-near infrared (UV-Vis-NIR) spectroscopy, X-ray diffraction (XRD), and field-emission scanning electron microscopy (FESEM). The analyses confirmed the successful incorporation of surface-bound ZIF-8 with low crystallinity, reduced bandgap energies (down to 3.07 eV), and mixed anatase-rutile phases. Using tetracycline as the target pollutant, the UV light photoactivity of the ZIF-8/TiO_2 composites was evaluated. Compared with commercial TiO_2, the composite prepared with 0.5 mM $Zn(NO_3)_2{\cdot}6H_2O$ and 4.0 mM $C_4H_6N_2$ (ZIF-8/TiO_2 (0.5,4.0)) exhibited enhanced photoactivity for tetracycline degradation (91.01%). These properties, including the high tetracycline photodegradation ability, make the ZIF-8/TiO_2 (0.5,4.0) photocatalyst a promising material for practical water treatment applications.

Keywords: Zeolitic imidazolate framework-8, Titania, Tetracycline, Photocatalyst, Photodegradation

1.0 Introduction

Tetracyclines are among the most widely prescribed antibiotics worldwide [1], yet they are poorly metabolized by humans and animals and cannot be effectively removed by conventional wastewater treatment plants (WWTPs) [2]. As a result, significant amounts of unmetabolized parent compounds and their degradation products are released into aquatic environments. For example, less than 70% of the parent tetracycline compound is metabolized, and approximately 21% is directly discharged into the environment after consumption [3]. The persistence of these residues poses growing ecological and public health concerns, driving intensive research into their toxicity, environmental fate, and degradation strategies [4]. Several methods, including physical, chemical, and biological approaches such as adsorption, membrane filtration, and prechlorination, have shown some effectiveness in treating tetracycline-containing solutions [1]. However, these methods still suffer from

drawbacks, including high maintenance requirements and operational cost [1]. Therefore, an effective and sustainable method for degrading tetracycline remains to be explored.

Photocatalysis has emerged as an efficient and sustainable approach for removing organic contaminants from wastewater [5]. Among various photocatalysts, titania (TiO_2) is one of the most extensively studied materials due to its strong oxidizing power, high photocatalytic activity, chemical stability, low cost, and non-toxicity [6]. As a light-activated catalyst, TiO_2 can effectively degrade a wide range of pollutants through the generation of electron-hole (e^--h^+) pairs under light irradiation. These charge carriers initiate redox reactions that produce reactive oxygen species (ROS), including hydroxyl radicals (•OH), and superoxide radicals ($•O_2^-$). These ROS are highly reactive and can oxidize organic pollutants, converting them into less harmful end products such as water, carbon dioxide, and inorganic ions [7]. However, the high recombination rate of photogenerated e^--h^+ pairs limits the overall photocatalytic efficiency by reducing the number of charge carriers available for photocatalytic reactions [8,9]. Therefore, suppressing the rate of e^--h^+ recombination is essential to enhance the photocatalytic performance of the TiO_2-based systems.

To overcome this limitation, different concentrations of zinc nitrate hexahydrate ($Zn(NO_3)_2·6H_2O$) and 2-methylimidazole ($C_4H_6N_2$) were used as precursors to synthesize zeolitic imidazolate framework-8/titania (ZIF-8/TiO_2) composites. The variation in precursor concentration plays a vital role in determining the formation and the structural characteristics of the ZIF-8 framework, which in turn determines its surface properties and photocatalytic performance [10]. ZIF-8 is a water-stable metal-organic framework (MOF) with a very high surface area that can effectively reduce the rate of e^--h^+ recombination and is widely used in adsorption, gas storage, catalysis, and other related fields [11]. Previous studies have demonstrated that MOFs can enhance photocatalytic performance in the degradation of organic pollutants [12–16]. Therefore, by defining suitable concentrations of $Zn(NO_3)_2·6H_2O$ and 2-methylimidazole, a synergistic effect between ZIF-8 and TiO_2 can be achieved, leading to enhanced photocatalytic degradation of tetracycline and other organic contaminants [17].

Hence, in this study, ZIF-8/TiO_2 composites were synthesized using different concentrations of $Zn(NO_3)_2·6H_2O$ and 2-methylimidazole. The physicochemical properties of the composites were characterized, and their UV light photocatalytic activity was evaluated through the degradation of tetracycline in aqueous solution. The findings offer valuable insights into high-efficiency photocatalysts and demonstrate promising potential for practical applications.

2.0 Materials and Method

2.1 Materials

Titanium(IV) oxide (TiO_2), zinc nitrate hexahydrate ($Zn(NO_3)_2·6H_2O$), and 2-methylimidazole ($C_4H_6N_2$) were supplied from Sigma Aldrich. Methanol (CH_3OH) and ethanol (C_2H_5OH) were purchased from Merck, and tetracycline was supplied by Alfa Aesar. All the materials were used without any further purification.

2.2 Preparation of ZIF-8/TiO_2 Composites

ZIF-8/TiO_2 composites were synthesized by incorporating TiO_2 into ZIF-8, following a modified procedure described elsewhere [18], and the effects of varying the amounts of $Zn(NO_3)_2·6H_2O$ and 2-methylimidazole were investigated. The schematic procedure is shown in Figure 1. Initially, 0.3g of TiO_2 was dispersed in methanol under ultrasonication for 30 minutes. Next, different amounts of $Zn(NO_3)_2·6H_2O$ were added to the solution under stirring for 20 minutes. The same amount of 2-methylimidazole (4.0 mM) was dissolved in 40 mL of methanol and stirred for 20 minutes. Then, the solution was slowly added to the former mixture and stirred at room temperature for 2 h. The obtained precipitate was collected by repeated centrifugation with methanol three times before drying at 70 °C for 12 h. The sample codes are listed in Table 1. The composites are designated as ZIF-8/TiO_2 (x,y), where x corresponds to the amount of $Zn(NO_3)_2·6H_2O$ and y is the amount of 2-methylimidazole used in the synthesis.

2.3 Characterization

Selected composites exhibiting the highest and lowest photocatalytic performance of tetracycline (see Section 3.5) were characterized using multiple techniques. The Fourier transform infrared (FTIR, Perkin-Elmer model 1600 Spectrometer) spectroscopy was used to determine the functional groups of the composites with a wavenumber ranging from 600 to 4000 cm^{-1}. Ultraviolet-visible-near infrared (UV-Vis-NIR, model UV-3600 PLUS Spectrophotometer) was used to measure and determine the bandgap energy of the samples at wavelengths 200 to 800 nm. To determine the crystallographic structure of the material, X-ray diffraction (XRD, Bruker AXS D8 Automatic Powder Diffractometer) with Cu Kα radiation (λ=1.54060 Å) was used with the scans in the 2θ range of 20 – 90 °. Lastly, the surface morphology and particle size distribution of the composites were investigated through field-emission scanning electron microscopy (FESEM, JEOL JSM-6701F) operated at 5.0 kV.

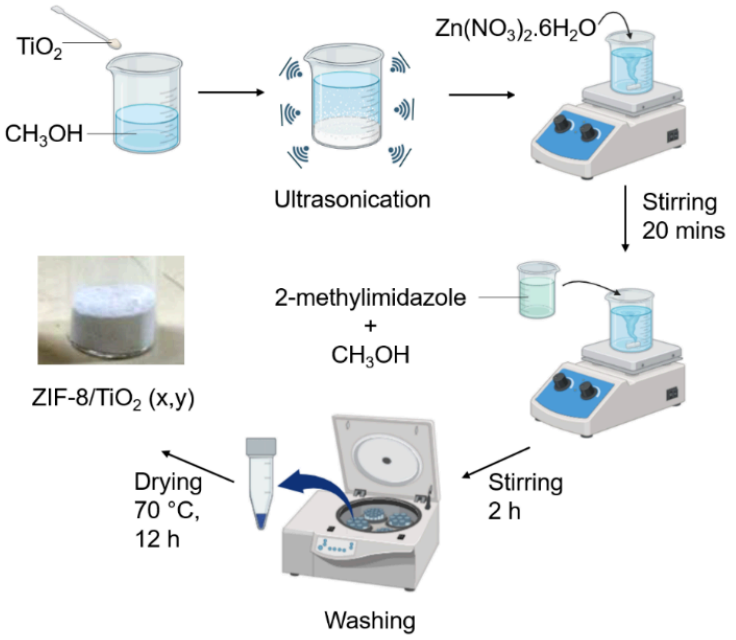

Figure 1 : Schematic of the ZIF-8/TiO_2 (x,y) composites synthesis process (x: amount of $Zn(NO_3)_2{\cdot}6H_2O$, y: amount of 2-methylimidazole).

Table 1: Coding of ZIF-8/TiO_2 composites prepared.

Sample code	$Zn(NO_3)_2{\cdot}6H_2O$ (mM)	$C_4H_6N_2$ (mM)
Effect of Different Amounts of $Zn(NO_3)_2{\cdot}6H_2O$		
ZIF-8/TiO_2 (0.5,4.0)	0.5	4.0
ZIF-8/TiO_2 (1.0,4.0)	1.0	4.0
ZIF-8/TiO_2 (2.0,4.0)	2.0	4.0
Effect of Different Amounts of $C_4H_6N_2$		
ZIF-8/TiO_2 (0.5,4.0)	0.5	4.0
ZIF-8/TiO_2 (0.5,8.0)	0.5	8.0
ZIF-8/TiO_2 (0.5,16.0)	0.5	16.0

2.4 Photocatalytic Degradation of Tetracycline

The photocatalytic activity was tested by the photodegradation of tetracycline in aqueous solution. 0.05 g of catalyst was added to 50 ml of 30 ppm tetracycline solution in a reaction tube. The mixture was stirred for 1 h in the dark in order to reach the adsorption-desorption equilibrium. The suspension was exposed to a 6 W lamp from Vilber Lourmat as the UV light source. 5 mL of tetracycline solution was taken out every 10 min till the end of the reaction, and its concentration was analyzed using a UV-Vis spectrophotometer (Shimadzu, UV-1800). The absorbance was measured at 354 nm with water as a reference. The photodegradation efficiency (%) of tetracycline was calculated as follows (Equation 1):

$$\text{Tetracycline photodegradation efficiency (\%)} = \frac{C_o - C_t}{C_o} \times 100\% \qquad \textbf{(Equation 1)}$$

Where C_o and C_t stand for the initial concentration of tetracycline and the concentration of tetracycline in real-time, respectively. The photocatalytic activity of the commercial TiO_2 was also measured under the same conditions as the reference. Figure 2 shows the setup for the photocatalytic reaction.

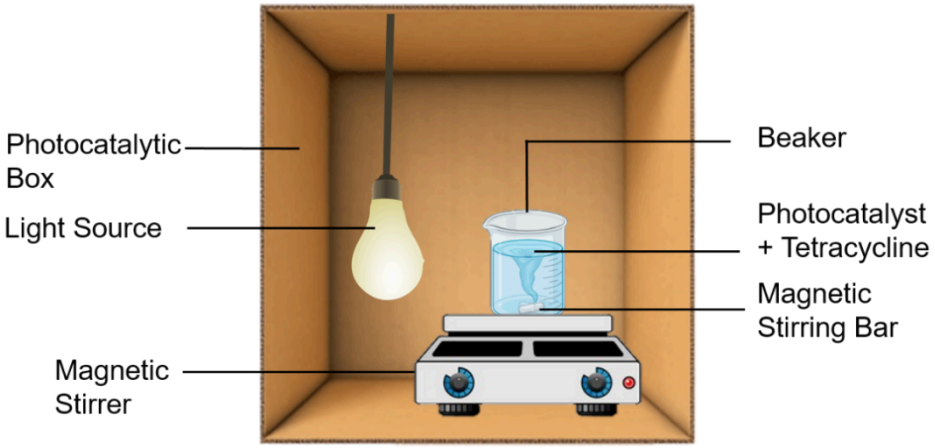

Figure 2 : Setup for the photocatalytic reaction.

3.0 Results and Discussion

3.1 Functional Group Analysis by FTIR Spectroscopy

The functional groups present in the TiO_2 and synthesized ZIF-8/TiO_2 composites were identified using FTIR spectroscopy. The FTIR spectra of ZIF-8 and the synthesized ZIF-8/TiO_2 composites are depicted in Figure 3. In the ZIF-8 spectrum (Figure 3a), the absorption peaks at 1098.27 cm^{-1} and 1384.16 cm^{-1} correspond to the C–N stretching and C–H bond bending vibrations, respectively. The peak at 156.57 cm^{-1} is ascribed to the C=N stretching, while the peak at 2926.97 cm^{-1} is attributed to the aliphatic C–H stretching of the imidazole ring [10,19]. Following the addition of ZIF-8 onto TiO_2 (Figure 3b-d), the absorption peaks from 600 to 800 cm^{-1} can be ascribed to the O–Ti–O bonds present in commercial TiO_2 [20]. A broad absorption band is observed at 3412.95 cm^{-1} (Figure 3b-d), which corresponds to the stretching vibration of O–H [21]. This band indicates the presence of adsorbed water molecules on the surface of TiO_2 particles. The observed structural changes and chemical bonding in the IR spectra indicate that the process of coupling ZIF-8 with TiO_2 to form composites was accomplished.

3.2 Bandgap Energy Determination by UV-Vis-NIR Spectroscopy

The UV-Vis-NIR absorption spectra analysis was used to determine the bandgap energy of the photocatalysts. Figure 4a shows the absorption spectra of ZIF-8 and ZIF-8/TiO_2 composites. The figure shows the blue shift in ZIF-8 absorption. ZIF-8 is known to have a significantly wide bandgap. The resulting ZIF-8 structure exhibits fewer electronic states within the bandgap when there are more Zn^{2+} ions present to properly interact with the 2-methylimidazole [22]. ZIF-8 has a shorter wavelength due to the wider bandgap, which causes a blue shift. ZIF-8/TiO_2 composites with 0.5 mM, 2.0 mM of $Zn(NO_3)_2{\cdot}6H_2O$, and 16.0 mM of 2-methylimidazole show shorter absorption wavelengths, indicating a smaller bandgap. Increasing the amounts of $Zn(NO_3)_2{\cdot}6H_2O$ shifted the absorption edge and slightly altered the bandgap [22]. The bandgap of ZIF-8/TiO_2 composites with 0.5 mM $Zn(NO_3)_2{\cdot}6H_2O$ exhibits a considerable shift, suggesting a small modification of the bandgap. ZIF-8/TiO_2 composites with 2.0 mM $Zn(NO_3)_2{\cdot}6H_2O$ exhibit a further shift, suggesting a more noticeable modification of the bandgap. The absorption edge shifts significantly when a greater amount of 2-methylimidazole (16.0 mM) is used. This shift is likely caused by modifications in the electronic structure between ZIF-8 and TiO_2 [23].

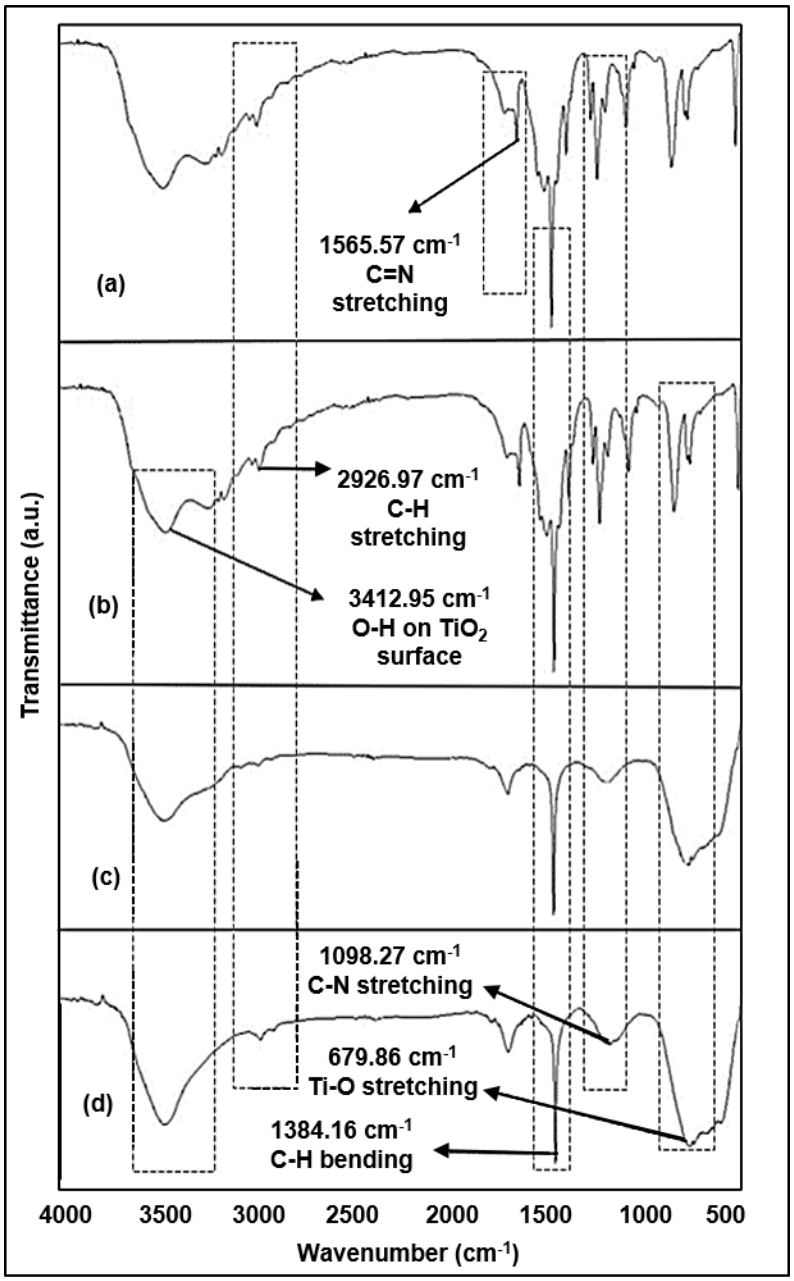

Figure 3 : FTIR spectra of (a) ZIF-8, (b) ZIF-8/TiO_2 (0.5,4.0), (c) ZIF-8/TiO_2 (2.0,4.0), and (d) ZIF-8/TiO_2 (0.5,16.0) composites.

The bandgap energy of the photocatalysts was calculated using the x-intercept value and linear extrapolation on the Tauc Plot of $(\alpha h\nu)^{1/2}$ against energy (hv), as shown in Figure 4b-e. A summary of the bandgap energy values for the produced photocatalysts has been listed in Table 2. According to Kanoun et al. (2024), commercial TiO_2 has a bandgap energy value of 3.2 eV, which suggests the presence of anatase phase TiO_2 [24]. The obtained bandgap energy values match the XRD data, suggesting that the samples are mainly in the anatase phase.

The data show that as the amounts of $Zn(NO_3)_2{\cdot}6H_2O$ increased from 0.5 mM to 2.0 mM, the bandgap of the composites decreased from 3.15 eV to 3.12 eV. This is most likely caused by small amounts of ZIF-8 forming on the TiO_2 surface, which can lower the overall bandgap by introducing new energy levels into the TiO_2 bandgap. The interaction between the metal centre (Zn) in the ZIF-8 structure and the organic linker (2-methylimidazole) results in these new energy levels [25]. These additional energy levels reduce the overall bandgap of TiO_2, thereby suppressing the encounter rate of photogenerated e^--h^+ pairs [26]. The incorporation of ZIF-8 plays a crucial role in enhancing its photocatalytic activity under UV light, effectively improving its overall efficiency in photocatalytic applications [27]. Furthermore, the bandgap of the composites decreased from 3.15 eV to 3.07 eV as the amount of 2-methylimidazole increased from 4.0 mM to 16.0 mM. More ZIF-8 forms on the TiO_2 surface when 2-methylimidazole is added in greater amounts (4.0 mM to 16.0 mM). More building

blocks are available for the development of ZIF-8 crystals on the TiO_2 surface due to the increased amounts of 2-methylimidazole. This improved interaction alters the electrical structure of the composite, contributing to a larger reduction in the bandgap [20]. The reduction in bandgap energy highlights the material's potential for photocatalytic applications under visible light irradiation, since a narrower bandgap extends the absorption edge toward longer wavelengths in the visible region.

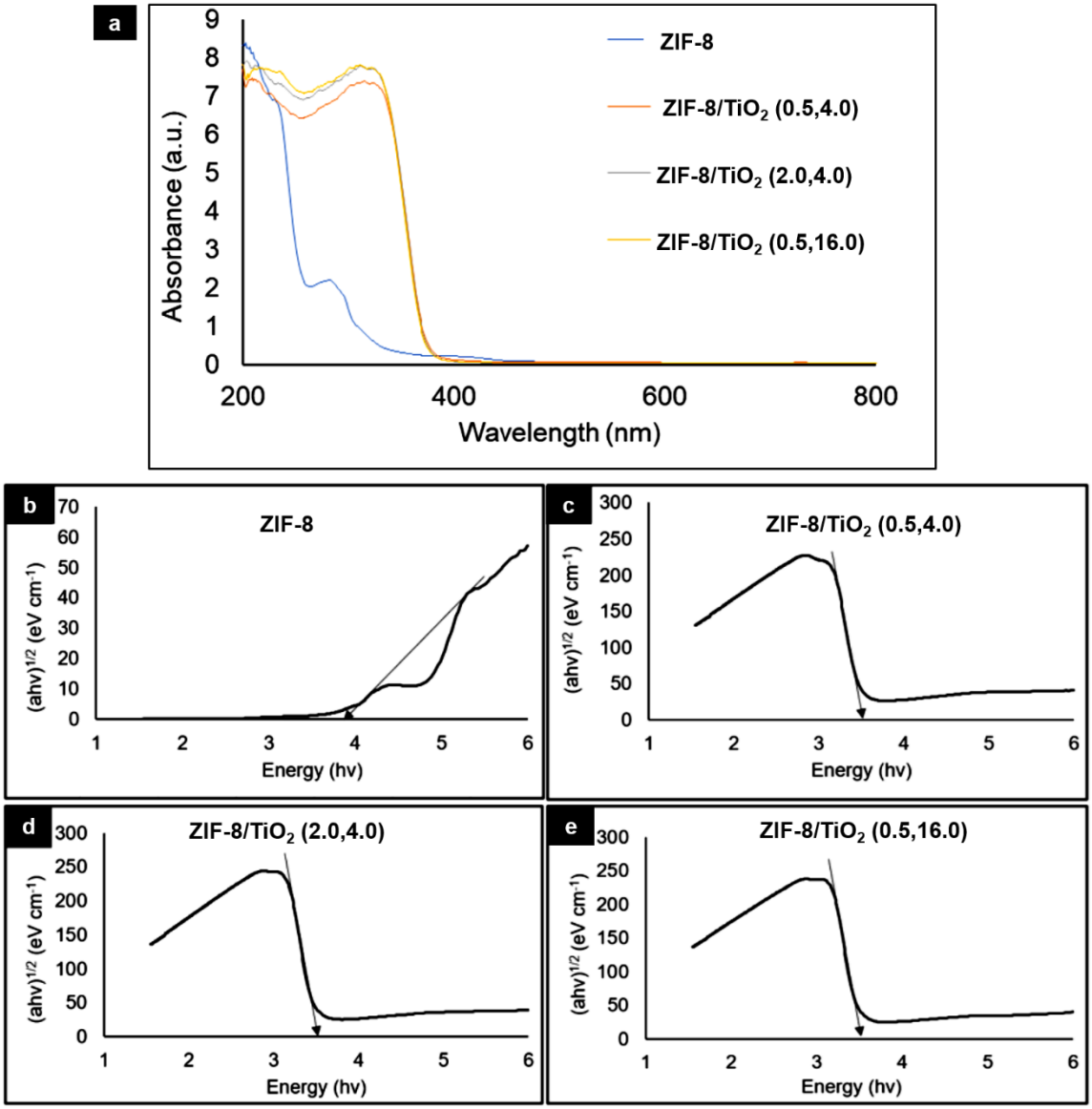

Figure 4 : (a) Absorption spectra of the photocatalysts obtained by UV-Vis-NIR spectroscopy and Tauc plots of (b) ZIF-8, (c) ZIF-8/TiO_2 (0.5,.0), (d) ZIF-8/TiO_2 (2.0,4.0), and (e) ZIF-8/TiO_2 (0.5,16.0) composites.

Table 2: Bandgap energy values of the photocatalysts.

Photocatalysts	Bandgap Energy (eV)
Commercial TiO_2	3.20
ZIF-8/TiO_2 (0.5,4.0)	3.15
ZIF-8/TiO_2 (2.0,4.0)	3.12
ZIF-8/TiO_2 (0.5,16.0)	3.07

3.3 Crystallinity Determination by XRD Analysis

Figure 5 shows the X-ray diffraction patterns of ZIF-8, ZIF-8/TiO_2 composites with 0.5 mM of $Zn(NO_3)_2{\cdot}6H_2O$, ZIF-8/TiO_2 composites with 2.0 mM of $Zn(NO_3)_2{\cdot}6H_2O$, and ZIF-8/TiO_2 composites with 0.5 mM of $Zn(NO_3)_2{\cdot}6H_2O$ and 16.0 mM of 2-methylimidazole. The figure shows different peaks for the crystalline planes of ZIF-8 and TiO_2 phases, indicating structural changes associated with the amounts of $Zn(NO_3)_2{\cdot}6H_2O$ and 2-methylimidazole. In ZIF-8/TiO_2 composites with 0.5 mM of $Zn(NO_3)_2{\cdot}6H_2O$, commercial TiO_2 diffraction peaks were observed at 2θ values of 37.50°, 47.71°, 53.59°, 54.72°, 62.38°, 69.95° and 74.74°. These values corresponded to the (004), (101), (112), (200), (105), (201), and (211) crystalline planes of anatase TiO_2, respectively. The values have a good correlation with the database of anatase TiO_2 as reported in the Joint Committee on Powder Diffractions (JCPDS 01- 075-2553). In addition, the rutile phase was found in the ZIF-8/TiO_2 composites with 0.5 mM of $Zn(NO_3)_2{\cdot}6H_2O$. The (110), (101), (204), and (214) crystalline phases of rutile TiO_2 are represented by the diffraction peaks that appear at 27.12°, 35.75°, 63.70°, and 76.02°, respectively.

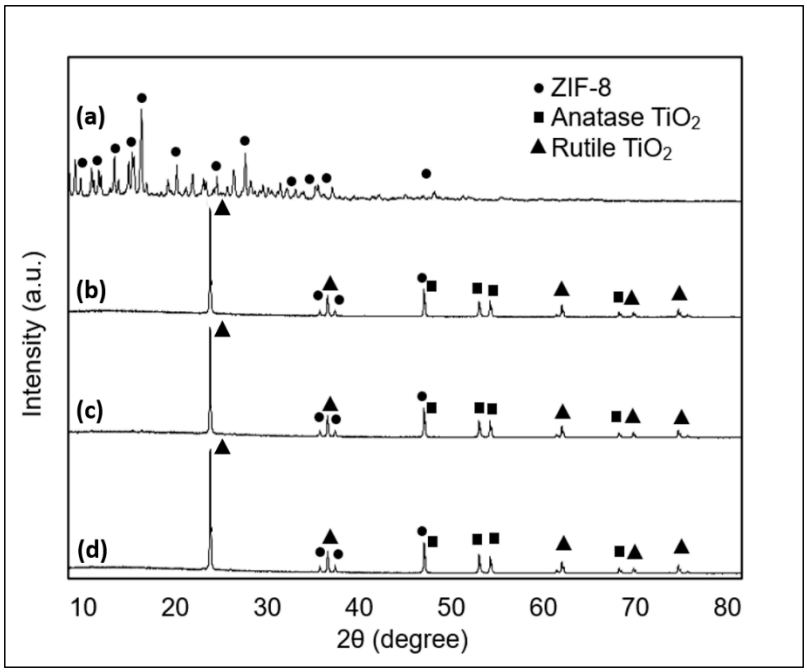

Figure 5 : XRD patterns of (a) ZIF-8, (b) ZIF-8/TiO_2 (0.5,4.0), (c) ZIF-8/TiO_2 (2.0,4.0), and (d) ZIF-8/TiO_2 (0.5,16.0) composites.

The peaks in the XRD patterns of ZIF-8/TiO_2 composites with 0.5 mM of $Zn(NO_3)_2{\cdot}6H_2O$ (Figure 5b), ZIF-8/TiO_2 composites with 2.0 mM of $Zn(NO_3)_2{\cdot}6H_2O$ (Figure 5c) and ZIF-8/TiO_2 composites with 16.0 mM of 2-methylimidazole (Figure 5d) samples are the same as those found in commercial TiO_2, while the characteristic peaks of ZIF-8 are weak. This observation is due to the surface-bound and low loading of ZIF-8 on TiO_2, which is consistent with previous reports on TiO_2/ZIF-8 composites [28]. The XRD pattern of ZIF-8 showed peaks at 2θ angles of 10.5°, 13.1°, 14.9°, 16.6°, 18.2°, 24.5°, 26.8°, 36.7°, 38.9°, 48.57° and 76.5° corresponding to ZIF-8 planes (100), (110), (002), (112), (121), (222), (233), (231), (223), (332) and (332) respectively. The highly crystalline structure of the ZIF-8 material is indicated by these distinct, sharp peaks [12]. A high level of crystallinity is indicated by these strong peaks, which show an organised and well-defined atom arrangement within the crystal lattice. The size and quality of the crystals are correlated with the sharpness of the peaks in the diffraction pattern, indicating that the method of synthesis, which promotes fewer nucleation centres, results in the development of larger, more uniform crystals.

The XRD results show that reducing the amounts of $Zn(NO_3)_2{\cdot}6H_2O$ and 2-methylimidazole leads to increased crystallinity and sharper peaks. This is because a smaller amount of reactants produces a more uniform and ordered arrangement of molecules within the crystal structure, resulting in a higher degree of crystallinity. This comprehensive study emphasizes how the amounts of 2-methylimidazole and $Zn(NO_3)_2{\cdot}6H_2O$ affect the structural properties of ZIF-8/TiO_2 composites, demonstrating the significance of XRD analysis in material characterization.

3.4 Morphological Studies and Elemental Composition by FESEM-EDX

The FESEM images of ZIF-8/TiO_2 composites are shown in Figure 6. Commercial TiO_2 nanoparticles showed agglomeration along with a uniform shape and spherical edges (Figure 6a). The TiO_2 agglomeration is visible at a magnification of 120,000. On the other hand, ZIF-8 (Figure 6b) has a polyhedron shape. After the formation of the composites, it can be clearly seen that the surfaces of the TiO_2 have been effectively coated with ZIF-8 particles, giving them a rougher morphology than the pure ZIF-8 particles (Figure 6c-e). TiO_2 and the ZIF-8 surface have a strong bond that keeps TiO_2 particles from aggregating and ensures their uniform dispersion.

The average particle sizes of the synthesized ZIF-8/TiO_2 composites and the commercial TiO_2 are summarized in Table 3. The commercial TiO_2 exhibited the smallest average particle size of 33.0 nm. In contrast, ZIF-8 showed a significantly larger average particle size of 105.1 nm, indicating larger grain growth compared to commercial TiO_2. Upon the formation of ZIF-8/TiO_2 composites, the average particle sizes increased relative to pure TiO_2, which can be attributed to the surface coverage of TiO_2 nanoparticles by ZIF-8 [13,29]. Compared to the ZIF-8/TiO_2 composites prepared with 0.5 mM of $Zn(NO_3)_2{\cdot}6H_2O$, the composites synthesized with 16.0 mM 2-methylimidazole exhibited a slightly larger average particle size. This increase may be attributed to the strong interfacial interaction between ZIF-8 and TiO_2, which effectively inhibits TiO_2 nanoparticles' agglomeration and promotes the formation of larger, well-defined composite structures [30]. However, among all the samples, the ZIF-8/TiO_2 composites prepared with 2.0 mM $Zn(NO_3)_2{\cdot}6H_2O$ showed the largest particle size. This is likely due to the reduced interfacial compatibility between the ZIF-8 and TiO_2 at this concentration, which may lead to decreased contact between TiO_2 nanoparticles and ZIF-8, resulting in particle growth and aggregation [31].

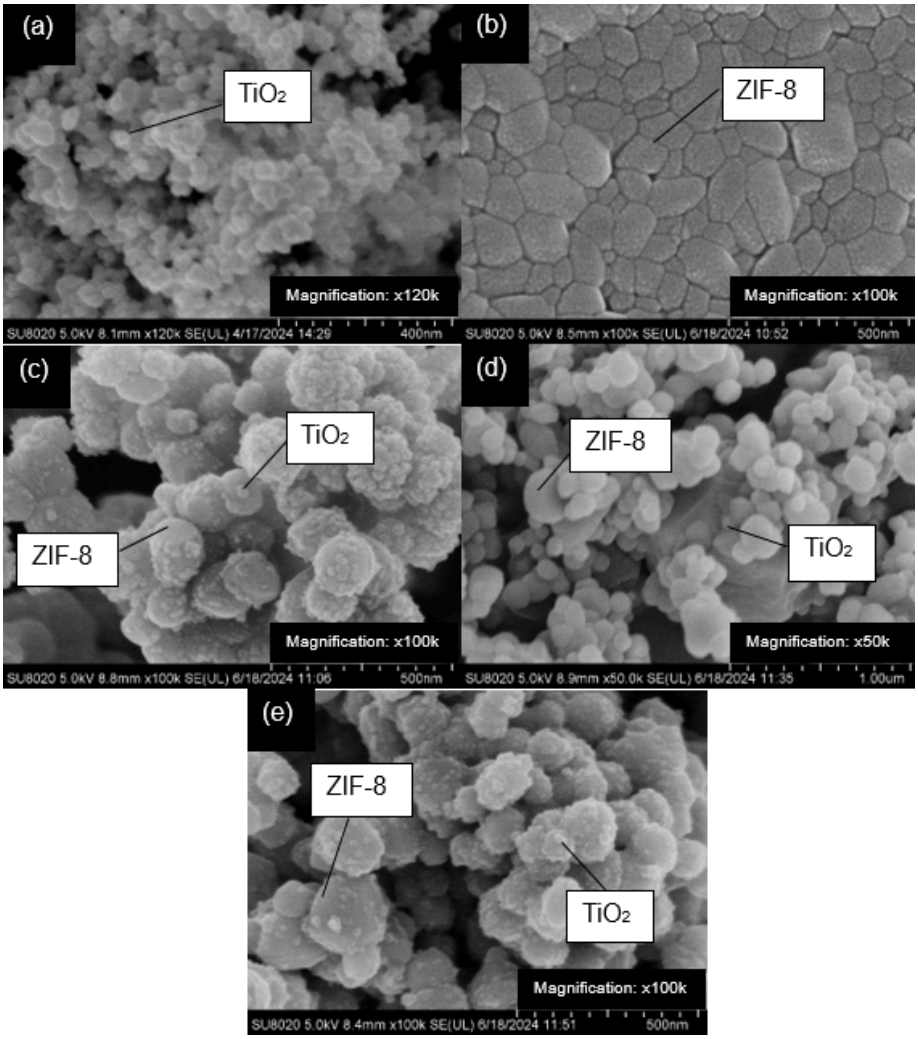

Figure 6 : FESEM images of (a) commercial TiO_2, (b) ZIF-8, (c) ZIF-8/TiO_2 (0.5,4.0), (d) ZIF-8/TiO_2 (2.0,4.0), and (e) ZIF-8/TiO_2 (0.5,16.0) composites.

Table 3: Average particle size of the photocatalysts.

Photocatalysts	Average particle sizes (nm)
Commercial TiO_2	33.0
ZIF-8	105.1
ZIF-8/TiO_2 (0.5,4.0)	92.5
ZIF-8/TiO_2 (2.0,4.0)	112.9
ZIF-8/TiO_2 (0.5,16.0)	108.3

The EDX analysis was carried out to confirm that ZIF-8/TiO_2 composites were successfully formed and to determine the elemental distribution of the synthesised samples. The synthesised materials are mostly made up of titanium (Ti), oxygen (O), carbon (C), nitrogen (N), and zinc (Zn). The presence of ZIF-8 in the samples explains the significant percentage of carbon found. Table 4 shows the atomic composition of the elements in the synthesised ZIF-8/TiO_2 composites based on the EDX analysis. In comparison to Ti, N, O, and Zn, all samples display the highest percentage of C species. This is because carbon atoms in the 2-methylimidazolate organic linkers coordinate with Zn^{2+} ions to produce ZIF-8. The amounts of $Zn(NO_3)_2{\cdot}6H_2O$ and 2-methylimidazole were changed, which resulted in variations in the percentage of Zn and N species between samples. A larger percentage of Zn and N species was obtained with higher amounts of $Zn(NO_3)_2{\cdot}6H_2O$ and 2-methylimidazole.

Table 4: The atomic composition of elements present in ZIF-8/TiO_2 composites.

Photocatalysts	Atomic Ratio (%)				
	Ti	O	C	Zn	N
Commercial TiO_2	25.1	74.9	-	-	-
ZIF-8	-	-	48.7	15.6	35.7
ZIF-8/TiO_2 (0.5,4.0)	8.5	29.3	62.0	0.2	-
ZIF-8/TiO_2 (2.0,4.0)	10.4	25.5	49.4	4.0	10.7
ZIF-8/TiO_2 (0.5,16.0)	28.5	23.4	67.5	0.5	-

3.5 Photocatalytic Degradation of Tetracycline

Figure 7 shows the degradation percentage of tetracycline treated with commercial TiO_2 and ZIF-8/TiO_2 composites using different amounts of $Zn(NO_3)_2{\cdot}6H_2O$ (0.5, 1.0, and 2.0 mM) with the same amount of 2-methylimidazole, which was 4.0 mM, after 1.5 h of UV light irradiation. Based on Figure 7, the commercial TiO_2 exhibits the lowest degradation percentage of 47.01%, indicating its limited efficiency under the tested conditions. Upon the addition of ZIF-8, a significant increase in the degradation percentage can be observed, which may be due to the formation of heterojunctions that facilitate charge transfer pathways and inhibit the recombination of e^--h^+ pairs [11,20].

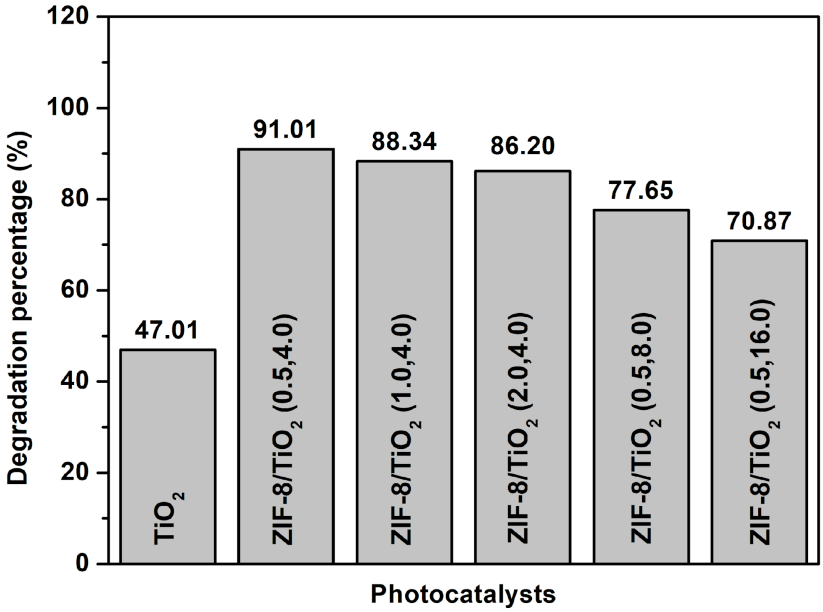

Figure 7 Degradation percentage of tetracycline under UV light irradiation by ZIF-8/TiO_2 photocatalysts.

Meanwhile, among all the tested photocatalysts, the ZIF-8/TiO_2 composite with 0.5 mM of $Zn(NO_3)_2{\cdot}6H_2O$ achieved the highest degradation percentage of tetracycline at 91.01%, followed by the composite with 1.0 mM of $Zn(NO_3)_2{\cdot}6H_2O$ at 88.34%, and the composite with 2.0 mM of $Zn(NO_3)_2{\cdot}6H_2O$ at 86.20%. The trend shows that a lower amount of $Zn(NO_3)_2{\cdot}6H_2O$, which is 0.5 mM, led to higher photocatalytic activity (ZIF-8/TiO_2 composites with 0.5 mM of $Zn(NO_3)_2{\cdot}6H_2O$. Better dispersion of Zn^{2+} ions inside the ZIF-8 structure can be caused by lower amounts of $Zn(NO_3)_2{\cdot}6H_2O$, which explains the increase in the photocatalytic degradation rate with the amounts of $Zn(NO_3)_2{\cdot}6H_2O$ [32].

The results also indicate that the increase in efficiency is attributed to the faster growth of the ZIF-8 structure and the improved interaction between ZIF-8 and TiO_2, which leads to enhanced photocatalytic activity [33]. However, at 1.0 mM and 2.0 mM, the degradation percentages slightly decrease to 88.34% and 86.2%, respectively. This reduction is most likely due to the formation of excess ZIF-8, which may cause aggregation or block the active sites on TiO_2, thereby limiting the overall efficiency [27,34].

As shown in Figure 7, among the ZIF-8/TiO_2 composites prepared with different concentrations of 2-methylimidazole, the highest degradation of tetracycline (91.01%) was achieved using 4.0 mM of 2-methylimidazole, followed by ZIF-8/TiO_2 composites with 8.0 mM (77.65%) and 16.0 mM (70.87%) under UV light irradiation. The photodegradation percentage decreased with increasing 2-methylimidazole concentration. This may be attributed to the excessive ZIF-8, which can more thoroughly cover the TiO_2's surface, thereby limiting the available active sites that are required for photocatalytic activity [18,31]. Furthermore, a high concentration of 2-methylimidazole may affect the crystallinity and morphology of ZIF-8. Inadequately crystalline or excessively dense ZIF-8 structures might not function effectively with TiO_2, resulting in poor interaction between the two elements. In contrast, at lower amounts of 2-methylimidazole (4.0 mM), the photodegradation percentage increases. The reduced amount of 2-methylimidazole may contribute to a more uniform and efficient catalyst distribution. Therefore, the amount of 2-methylimidazole plays a crucial role in determining the photodegradation efficiency of the ZIF-8/TiO_2 composite photocatalyst.

4.0 Conclusion

In this study, ZIF-8/TiO_2 composites were successfully synthesized, and the influence of synthesis parameters on their physicochemical properties and photocatalytic performance was systematically investigated. Despite appearing as low-crystallinity in XRD, ZIF-8 was effectively formed on the TiO_2 surface and played a functional role in enhancing photocatalytic activity. Among all samples, ZIF-8/TiO_2 (0.5, 4.0) achieved the highest degradation efficiency (91.01%), due to optimal surface dispersion of ZIF-8 that suppressed electron-hole recombination without excessively blocking TiO_2 active sites. These findings confirm that even at low-crystallinity ZIF-8 layers can significantly improve the photocatalytic performance of TiO_2-based photocatalyst.

Acknowledgement

The authors gratefully acknowledge funding provided by Universiti Teknologi Malaysia from Geran Penyelidikan Hi-Tech (F4) (Q.J130000.4654.00Q19) and PDRUS Grant Vote No. 07E44.

References

[1] Amangelsin, Y., Semenova, Y., Dadar, M., Aljofan, M., & Bjorklund, G. (2023). The impact of tetracycline pollution on the aquatic environment and removal strategies. *Antibiotics*, *12*(3), 1–15. https://doi.org/10.3390/antibiotics12030440
[2] Zhang, L., Zhu, Z., Zhao, M., He, J., Zhang, X., Hao, F., & Du, P. (2023). Occurrence, removal, emission and environmental risk of 32 antibiotics and metabolites in wastewater treatment plants in Wuhu, China. *Science of the Total Environment*, *899*, 1–10. https://doi.org/10.1016/j.scitotenv.2023.165681
[3] Yang, Q., Gao, Y., Ke, J., Show, P. L., Ge, Y., Liu, Y., Guo, R., & Chen, J. (2021). Antibiotics: An overview on the environmental occurrence, toxicity, degradation, and removal methods. *Bioengineered*, *12*(1), 7376–7416. https://doi.org/10.1080/21655979.2021.1974657
[4] Verdini, F., Calcio Gaudino, E., Canova, E., Colia, M. C., & Cravotto, G. (2023). Highly efficient tetracycline degradation under simultaneous hydrodynamic cavitation and electrical discharge plasma in flow. *Industrial & Engineering Chemistry Research*, *14*, 1–6. https://doi.org/10.1021/acs.iecr.3c00266
[5] Naghizadeh, A., Etemadinia, T., Derakhshani, E., & Esmati, M. (2023). Graphitic carbon nitride loaded on powdered mesoporous silica nanoparticles for photocatalytic tetracycline antibiotic degradation under UV-C light irradiation. *Research on Chemical Intermediates*, *49*(3), 1165–1177. https://doi.org/10.1007/s11164-022-04942-z
[6] AbdulKareem, E. A., Mahmoud, Z. H., & Khadom, A. A. (2023). Sunlight assisted photocatalytic mineralization of organic pollutants over RGO impregnated TiO2 nanocomposite: Theoretical and experimental study. *Case Studies in Chemical and Environmental Engineering*, *8*, 1–14. https://doi.org/10.1016/j.cscee.2023.100446
[7] Al Miad, A., Saikat, S. P., Alam, M. K., Sahadat Hossain, M., Bahadur, N. M., & Ahmed, S. (2024). Metal oxide-based photocatalysts for the efficient degradation of organic pollutants for a sustainable environment: A review. *Nanoscale Advances*, *6*, 4781–4803. https://doi.org/10.1039/d4na00517a

[8] Suhaimi, N. H. S., Azhar, R., Adzis, N. S., Mohd Ishak, M. A., Ramli, M. Z., Hamzah, M. Y., Ismail, K., & Nawawi, W. I. (2025). Recent updates on TiO2-based materials for various photocatalytic applications in environmental remediation and energy production. *Desalination and Water Treatment*, *321*, 1–22. https://doi.org/10.1016/j.dwt.2024.100976
[9] El Mchaouri, M., Mallah, S., Abouhajjoub, D., Boumya, W., Elmoubarki, R., Essadki, A., Barka, N., & Elhalil, A. (2025). Engineering TiO2 photocatalysts for enhanced visible-light activity in wastewater treatment applications. *Tetrahedron Green Chemistry*, *6*, 1–21. https://doi.org/10.1016/j.tgchem.2025.100084
[10] Gao, J., Chu, W., Ding, X., Ding, L., Guo, Q., & Fu, Y. (2023). Degradation kinetic studies of BSA@ZIF-8 nanoparticles with various zinc precursors, metal-to-ligand ratios, and pH conditions. *ACS Omega*, *8*(47), 44601–44610. https://doi.org/10.1021/acsomega.3c04973
[11] Li, R., Li, W., Jin, C., He, Q., & Wang, Y. (2020). Fabrication of ZIF-8@TiO2 micron composite via hydrothermal method with enhanced absorption and photocatalytic activities in tetracycline degradation. *Journal of Alloys and Compounds*, *825*, 2–11. https://doi.org/10.1016/j.jallcom.2020.154008
[12] Angela, S., Lunardi, V. B., Kusuma, K., Soetaredjo, F. E., Putro, J. N., Santoso, S. P., Angkawijaya, A. E., Lie, J., Gunarto, C., Kurniawan, A., & Ismadji, S. (2021). Facile synthesis of hierarchical porous ZIF-8@TiO2 for simultaneous adsorption and photocatalytic decomposition of crystal violet. *Environmental Nanotechnology, Monitoring & Management*, *16*, 1–14. https://doi.org/10.1016/j.enmm.2021.100598
[13] Jing, Y., Yin, H., Li, C., Chen, J., Wu, S., Liu, H., Xie, L., Lei, Q., Sun, M., & Yu, S. (2022). Fabrication of Pt doped TiO2–ZnO@ZIF-8 core–shell photocatalyst with enhanced activity for phenol degradation. *Environmental Research*, *203*, 1–6. https://doi.org/10.1016/j.envres.2021.111819
[14] Cen, L., Tang, T., Yu, F., Wu, H., Li, C., Zhu, H., & Guo, Y. (2023). Fabrication of ZIF-8/TiO2 electrospinning nanofibers for synergistic photodegradation in dyeing wastewater. *Journal of Industrial and Engineering Chemistry*, *126*, 537–545. https://doi.org/10.1016/j.jiec.2023.06.042
[15] Wang, T., Li, M., Wang, W., Liu, X., Qi, X., Su, X., Shi, D., Zhan, H., & Wang, Y. (2024). Preparation of TiO2(B)/GO/ZIF-8 with enhanced photocatalytic performance for ibuprofen degradation under visible light. *Materials Science and Engineering: B*, *301*, 1–8. https://doi.org/10.1016/j.mseb.2023.117163
[16] Tamimzadeh, A., Dodelehband, A., Gordanshekan, A., Arabian, S., Farahmand, R., Farhadian, M., Solaimany Nazar, A. R., & Tangestaninejad, S. (2025). A multifaceted investigation on photocatalytic performance of Bi2WO6/TiO2/ZIF-8: Adsorption, artificial neural networks, density functional theory, and antibacterial assessment studies. *Advanced Powder Technology*, *36*(8), 1–17. https://doi.org/10.1016/j.apt.2025.104984
[17] Trung, L. G., Nguyen, M. K., Hang Nguyen, T. D., Tran, V. A., Gwag, J. S., & Tran, N. T. (2023). Highly efficient degradation of reactive black KN-B dye by ultraviolet light responsive ZIF-8 photocatalysts with different morphologies. *RSC Advances*, *13*(9), 5908–5924. https://doi.org/10.1039/d2ra08312d
[18] Zhang, Y., Jia, Y., Li, M., & Hou, L. (2018). Influence of the 2-methylimidazole/zinc nitrate hexahydrate molar ratio on the synthesis of zeolitic imidazolate framework-8 crystals at room temperature. *Scientific Reports*, *8*(1), 1–8. https://doi.org/10.1038/s41598-018-28015-7
[19] Zhu, Y., Zhi, Q., Zhang, C., Gu, Y., Liu, S., Qiao, S., & Lai, H. (2023). Debridement of contaminated implants using air-polishing coupled with pH-responsive Maximin H5-embedded metal–organic frameworks. *Frontiers in Bioengineering and Biotechnology*, *11*, 1–14. https://doi.org/10.3389/fbioe.2023.1124107
[20] Yurtsever, H. A., & Çetin, A. E. (2021). Fabrication of ZIF-8-decorated copper-doped TiO2 nanocomposite at low ZIF-8 loading for solar energy applications. *Colloids and Surfaces A: Physicochemical and Engineering Aspects*, *625*, 1–10. https://doi.org/10.1016/j.colsurfa.2021.126980
[21] Gabriela, R. N., Heryanto, H., & Tahir, D. (2025). Nanocomposite TiO2/ZnO/chitosan by sol-gel method for self-cleaning application. *International Journal of Biological Macromolecules*, *298*, 140076. https://doi.org/10.1016/j.ijbiomac.2025.140076
[22] Tahir, M. B., Sohaib, M., Sagir, M., & Rafique, M. (2021). Role of nanotechnology in photocatalysis. *Encyclopedia of Smart Materials*, *2*, 578–589. https://doi.org/10.1016/B978-0-12-815732-9.00006-1
[23] Khalilova, H. K., Hasanova, S. A., & Aliyev, F. G. (2018). Photocatalytic removal of organic pollutants from industrial wastewater using TiO2 catalyst. *Journal of Environmental Protection*, *9*(6), 691–698. https://doi.org/10.4236/jep.2018.96043
[24] Kanoun, M. B., Ahmed, F., Awada, C., Jonin, C., & Brevet, P. F. (2024). Band gap engineering of Au doping and Au–N codoping into anatase TiO2 for enhancing visible-light photocatalytic performance. *International Journal of Hydrogen Energy*, *51*, 907–913. https://doi.org/10.1016/j.ijhydene.2023.10.244
[25] Pouramini, Z., Mousavi, S. M., Babapoor, A., Hashemi, S. A., & Lai, C. W. (2023). Effect of metal atoms in zeolitic imidazolate frameworks (ZIF-8 & 67) for removal of dyes and antibiotics from wastewater: A review. *Catalysts*, *13*(1), 155. https://doi.org/10.3390/catal13010155
[26] Ökte, A. N., & Tuncel, D. (2025). TiO2@ZIF-8 hybrid as a type II heterojunction photocatalyst: Adsorption/photocatalytic properties, kinetics, and effect of humidity. *Photochemical & Photobiological Sciences*, *24*(7), 1107–1126. https://doi.org/10.1007/s43630-025-00754-3
[27] Xia, T., Lin, Y., Li, W., & Ju, M. (2021). Photocatalytic degradation of organic pollutants by MOFs-based materials: A review. *Chinese Chemical Letters*, *32*(10), 2975–2984. https://doi.org/10.1016/j.cclet.2021.02.058
[28] Zou, Y., & Wang, H. (2021). Self-assembly of TiO2/ZIF-8 nanocomposites for varied photocatalytic CO2 reduction with H2O vapor induced by different synthetic methods. *Nanoscale Advances*, *3*, 1455–1463. https://doi.org/10.1039/d0na00814a
[29] Zeng, X., Huang, L., Wang, C., Wang, J., Li, J., & Luo, X. (2016). Sonocrystallization of ZIF-8 on electrospinning TiO2 nanofibers surface with enhanced photocatalysis property through synergistic effect. *ACS Applied Materials & Interfaces*, *8*(31), 20274–20282. https://doi.org/10.1021/acsami.6b05746
[30] Zhang, Y., Li, Q., Liu, C., Shan, X., Chen, X., Dai, W., & Fu, X. (2018). The promoted effect of ZIF-8 on Au/TiO2 for CO oxidation at room temperature in dark and under visible light irradiation. *Applied Catalysis B: Environmental*, *224*, 283–294. https://doi.org/10.1016/j.apcatb.2017.10.027
[31] Bogdan, L., & Pal, A. (2023). Eco-friendly synthesis of TiO2/ZIF-8 composites: Characterization and application for the removal of imidacloprid from wastewater. *Processes*, *11*, 963. https://doi.org/10.3390/pr11030963
[32] Amani, S., Rostamizadeh, M., & Ghadimi, A. (2021). Highly active Fe-doped ZIF-8 nanocatalyst in electrochemical degradation of pharmaceutical pollutant in neutral environment. *Journal of Water and Environmental Nanotechnology*, *6*(2), 138–149. https://doi.org/10.22090/jwent.2021.02.004
[33] Safeen, A., Safeen, K., Ullah, R., Zulfqar, N., Shah, W. H., Zaman, Q., Althubeiti, K., Al Otaibi, S., Rahman, N., Iqbal, S., Khan, A., Khan, A., & Khan, R. (2022). Enhancing the physical properties and photocatalytic activity of TiO2 nanoparticles via cobalt doping. *RSC Advances*, *12*(25), 15767–15774. https://doi.org/10.1039/d2ra01948e

[34] Arora, I., Chawla, H., Chandra, A., Sagadevan, S., & Garg, S. (2022). Advances in strategies for enhancing photocatalytic activity of TiO2: Conversion from UV-light active to visible-light active photocatalyst. *Inorganic Chemistry Communications*, *143*, 1–20. https://doi.org/10.1016/j.inoche.2022.109700